Modeling of Cardiac Component of Subarachnoid Space Changes in Apnoea Resulting as a Function of Blood Pressure and Blood Flow Parameters

Two Mechanizm of Regulation

Kamila Mazur[1], Renata Kalicka[1], Andrzej F. Frydrychowski[2] and Pawel J. Winklewski[2]
[1]*Department of Biomedical Engineering, Faculty of Electronics, Telecommunications and Informatics, Gdańsk University of Technology, Narutowicza 11/12, Gdańsk, Poland*
[2]*Institute of Human Physiology, Medical University of Gdansk, Gdansk, Poland*

Keywords: Subarachnoid Space Width, Pial Artery, Brain Haemodynamics, Apnea, NIR-T/BSS.

Abstract: Experiments were performed in a group of 19 healthy, non-smoking volunteers. The experiment consisted of three apnoeas, sequentially: 30 s apnoea, 60 s apnoea and maximal, that could be done, apnoea. The breath-hold was separated for 5 minutes rest. The following parameters were measured and obtained for further analysis: blood parameters, artery diameter of the internal carotid artery, end-tidal CO_2 in expired air, the cardiac (from 0.5 to 5.0 Hz) and slow (< 0.5 Hz) components of subarachnoid space width signal. As a result of the experiment, we observed two different reactions, using the same experimental procedure. It seemed to indicate two different operating modes and two separate models. As a consequence, there are two subsets of slow subarachnoid space width responses to breath-hold in humans. A positive subarachnoid space width changes (slow) component depends on changes in heart rate, pulsatility index and cerebral blood flow velocity. A negative subarachnoid space width changes component is driven by heart rate changes and pulsatility index changes. The different heart-generated arterial pulsation response to experimental breath-hold provides new insights into our understanding of the complex mechanisms governing the adaptation to apnoea in humans. We propose a mathematical methodology that can be used in further clinical research.

1 INTRODUCTION

In medicine, there is an unmet need for continuous monitoring of subarachnoid space (SAS) width changes. The subarachnoid space (subarachnoid cavity) is a part of the central nervous system. It is small region on the surface of the hemispheres of the brain (the anatomic space between the arachnoid mater and the pia mater). It is filled by the cerebrospinal fluid (the same is in the spinal cord). The subarachnoid space is the location of the interface between the vascular tissue and the cerebrospinal fluid and is active in the blood brain barrier (Drake et al., 2009), (Winklewski et al., 2013), (Winklewski, 2015), (Wszedybyl-Winklewska et al., 2015).

Some efforts are undertaken to link changes in SAS width with changes in pressure and speed of blood. Showing signs of future success, is direction of research using results obtained by near-infrared transillumination/backscattering sounding, i.e. NIR-T/BSS. This is new, non-invasive method, which allows to assessment of pial artery pulsation (it is based on infrared radiation IR). In contrast to near-infrared spectroscopy (NIRS), which relies on the absorption of IR by haemoglobin, NIR-T/BSS uses the subarachnoid space (SAS), which is filled with translucent cerebrospinal fluid, as a propagation duct for IR. Thus, NIR-T/BSS allows continuous observation of SAS width changes (Winklewski et al., 2015c).

The whole NIR-T/BSS signal (TQ) was expressed in form of two components: a fast - the cardiac component (ccTQ) and a slow - the subarachnoid space component (sasTQ) (Frydrychowski et al., 2002), (Frydrychowski and Plucinski, 2007).

Mazur K., Kalicka R., Frydrychowski A. and Winklewski P.
Modeling of Cardiac Component of Subarachnoid Space Changes in Apnoea Resulting as a Function of Blood Pressure and Blood Flow Parameters - Two Mechanizm of Regulation.
DOI: 10.5220/0006139901400147
In *Proceedings of the 10th International Joint Conference on Biomedical Engineering Systems and Technologies (BIOSTEC 2017)*, pages 140-147
ISBN: 978-989-758-214-1

The subject of interest in the paper is a dependence between the cardiac component (ccTQ), subarachnoid space component (sasTQ) and blood parameters observed in apnoea experiment. This dependence allowed to model ccTQ or sasTQ as a function of cardiac parameters.

2 MATERIALS AND METHODS

The experimental protocol and the study were approved by the Ethics Committee of the Medical University of Gdansk (NKEBN/48/2011). Experiments were performed in a group of 20 healthy, nonsmoking volunteers. One of the volunteers was rejected on formal grounds and the results from 19 volunteers have been analyzed. All individuals gave written informed consent to participate in the study. Nicotine, coffee, tea, cocoa and methylxanthine- containing food and beverages were not permitted for 8 h before the tests. In addition, prior to each test, the volunteers were asked to rest comfortably for 30 min in the supine position. To avoid any air leakage during the experiment, individuals were equipped with a nose clip and were instructed to hold their lips closed. Each apnea was initiated at the end-phase of a normal inspiration, and a special emphasis was put on avoiding enhanced inspiration. In addition, individuals were asked not to hyperventilate before each apnea testing.

Experiment consist of 3 following apnoeas: 30s breath-hold, 60s breath-hold and maximal breath-hold. Apneas were separated by 5 min rest intervals.

The following signals were measured:

- ccTQ - changes in the cardiac component of SAS oscillations, resulting from heart-generated arterial pulsation (from 0.5 to 5.0 Hz) by NIR-T/BSS with a headmounted SAS 100 Monitor (NIRTI SA; Wierzbice, Poland);
- sasTQ - changes in slow component (< 0.5 Hz) of SAS oscillations by NIR-T/BSS with a headmounted SAS 100 Monitor (NIRTI SA; Wierzbice, Poland);
- SP and DP - systolic and diastolic blood pressure by Finometer; Finapres Medical Systems, Arnhem, the Netherlands;
- HR - heart rate by Finometer; Finapres Medical Systems, Arnhem, the Netherlands;
- CBFV - mean cerebral blood flow velocity in the internal carotid artery by Doppler ultrasound (Vivid 7; GE Healthcare; Little Chalfont, UK);
- RI - resistivity index of the internal carotid artery by Doppler ultrasound (Vivid 7; GE Healthcare; Little Chalfont, UK)
- PI - pulsatility index of the internal carotid artery by Doppler ultrasound (Vivid 7; GE Healthcare; Little Chalfont, UK);
- d - artery diameter of the internal carotid artery by Doppler ultrasound (Vivid 7; GE Healthcare; Little Chalfont, UK);
- SaO_2 - blood oxygen saturation by ear-clip sensor Massimo Oximeter; Massimo, Milano, Italy;
- $EtCO_2$ - the end-tidal CO_2 in expired air by a mouthpiece gas analyzer (PNT Digital M.E.C. Group, Brussels, Belgium.

The measurements were used to calculate mean arterial pressure (MAP) defined as weighted mean of the systolic (SP) and diastolic (DP) blood pressure during a single cardiac cycle (Kaźmierski, 2011):

$$\mathrm{MAP} = \frac{\mathrm{SP} + 2 \cdot \mathrm{DP}}{3} \tag{1}$$

During the experiment, the measurements were taken in 4 time points (except of $EtCO_2$ and d, which were measured only twice): t1 - baseline measurement, t2 - start of apnoea measurement, t3 - end of apnoea measurement and t4 - recovery measurement. The time points form the vector **t:**

$$\mathbf{t} = [t1, t2, t3, t4] = [tj\ ], j = 1,2,3,4 \tag{2}$$

All parameters, measured and calculated, were arranged in the form of parameter vector **w:**

$$\begin{aligned} \mathbf{w} &= [\mathrm{ccTQ}, \mathrm{sasTQ}, \mathrm{SP}, \mathrm{DP}, \mathrm{MAP}, \mathrm{HR}, \mathrm{CBFV}, \mathrm{RI}, \\ &\quad \mathrm{PI}, \mathrm{d}, \mathrm{SaO_2}, \mathrm{EtCO_2}] \\ \mathbf{w} &= [w_1, w_2, w_3, w_4, w_5, w_6, w_7, w_8, \\ &\quad w_9, w_{10}, w_{11}, w_{12}] = \\ &= [w_i], i = 1,2,...,12 \end{aligned} \tag{3}$$

The parameters were obtained for 19 patients in 3 different apnoeas, so we analyzed 57 different cases.

To observe the dynamics of w_i change, the differences between parameters value measured in two time points of experiment, i.e. w_i^{tj} and $w_i^{t\xi}$, were analysed. To choose the most significant change the $\Delta_{j\xi} w_i$, it was required to determine the pair of experiment time points, which is the most informative. Due to, the null hypothesis H_0 was developed:

$$H_0 : \overset{mean}{w_i^{tj}} = \overset{mean}{w_i^{t\xi}}, \quad j = 1,2,3,4 \wedge \xi = 2,3,4 \wedge \xi > j \tag{4}$$

for normally distributed w_i (the t-test was used), and:

$$H_0 : \overset{median}{w_i^{tj}} = \overset{median}{w_i^{t\xi}}, \quad j = 1,2,3,4 \wedge \xi = 2,3,4 \wedge \xi > j \tag{5}$$

for not normally distributed w_i (the Wilcoxon test was used). The normal distribution of data was tested by Shapiro-Wilk test (Kalicka, 2014).

The testing results are presented in Table 1. The Table 1 shows that differences between the baseline measurement and the end of apnoea measurement are the most informative. So, we analysed new data set: $\Delta_{13}w_i = w_i^3 - w_i^1$. Spearman's rank correlation analysis proved that it is possible to create a model for Δ_{13}ccTQ in form of mathematical, monotonic relationship. The coefficient of determination R^2 ranges from 0.4 to 0.6. The functional dependence was a moderately good. Still we were looking for a better functional relationship.

Next step was clustering. Cluster analysis is the task of grouping a set of objects in such way that objects in the same group (cluster) are more similar (in some sense or another) to each other than to those in other groups (clusters) (Everitt et al., 2001).

One of agglomerative hierarchical clustering method is complete linkage clustering. At the beginning of this method, each element is in a cluster of its own. The clusters are then sequentially combined into larger clusters until all elements end up being in the same cluster. At each step, the two clusters separated by the shortest distance are combined. The definition of 'shortest distance' is what differentiates between the different agglomerative clustering methods (for example Chebyshev distance). In complete-linkage clustering, the link between two clusters contains all element pairs, and the distance between clusters equals the distance between those two elements (one in each cluster) that are farthest away from each other. The shortest of these links that remains at any step causes the fusion of the two clusters whose elements are involved. The method is also known as farthest neighbour clustering. The result of the clustering can be visualized as a dendrogram (see Figure 1), which shows the sequence of cluster fusion and the distance at which each fusion took place (Everitt et al., 2001), (Stanisz, 2007).

For separation data in data set was used complete linkage with Chebyshev distance. Based on this agglomerative hierarchical clustering method (see Figure 1), Δ_{13}ccTQ was divided into two groups:

- left cluster: all situated on the left side on cluster analysis tree diagram, further referred to as $\Delta_{13}ccTQ^{\text{left cluster}}$;
- right cluster: all situated on the right side on cluster analysis tree diagram, further referred to as $\Delta_{13}ccTQ^{\text{right cluster}}$.

We took a guess that the groups should be considered separately. Two different reactions for the same course of experiment seem to indicate two different operating modes and two different models.

Two different models were designed (to validate the coefficient of determination was used): for left cluster $\Delta_{13}ccTQ^{\text{left cluster}}$ and for right cluster $\Delta_{13}ccTQ^{\text{right cluster}}$.

When $R^2>0.7$ the functional dependence is said to be very good (Kalicka, 2013).

3 RESULTS

The results of the Wilcoxon test (for not normally distributed w_i) and t-test (for normally distributed w_i) are presented in Table 1. Pairs of w_i which are statistically significant are in shaded cells.

The Table 1 shows that differences between the baseline measurement and the end of apnoea measurement are the most informative. So, we analysed new data set: $\Delta_{13}w_i = w_i^3 - w_i^1$.

Based on the cluster analysis (complete linkage, Chebyshev distance, see Figure 1), Δ_{13}ccTQ was divided into two groups:

- left cluster $\Delta_{13}ccTQ^{\text{left cluster}}$, where Δ_{13}sasTQ<0, contained 29 cases under test
- right cluster $\Delta_{13}ccTQ^{\text{right cluster}}$, where Δ_{13}sasTQ>0, contained 22 cases under test.

Six cases were rejected as impossible to classify.

Two different models were designed and two coefficients of determination were obtained:

- $R^2=0.7579$ for $\Delta_{13}ccTQ^{\text{left cluster}}$,
- $R^2=0.7007$ for $\Delta_{13}ccTQ^{\text{right cluster}}$.

Coefficient of determination was $R^2>0.7$, so the models were satisfactory.

Table 1: Statistical significance level p between w_i^{tj} and $w_i^{t\xi}$. For normally distributed measurements t-test was applied, otherwise when normal distribution condition was not satisfied, the Wilcoxon test was used (W test). Pairs of w_i which are statistically significant are in shaded cells.

	baseline measurement → start of apnea measurement t1→t2	***baseline measurement → end of apnea measurement t1→t3***	***baseline measurement → recovery measurement t1→t4***	***start of apnea measurement → end apnea measurement t2→t3***	***start of apnea measurement → recovery measurement t2→t4***	***end of apnea measurement → recovery measurement t3→t4***
w_1 (ccTQ)	W test *p<0.01*	W test *p<0.01*	W test *p<0.01*	W test *p>0.01*	W test *p<0.01*	W test *p>0.01*
w_2 (sasTQ)	W test *p<0.01*	W test *p>0.01*	W test *p>0.01*	W test *p<0.01*	W test *p<0.01*	W test *p<0.01*
w_3 (SP)	t-test *p<0.01*	t-test *p<0.01*	t-test *p>0.01*	t-test *p<0.01*	t-test *p<0.01*	t-test *p<0.01*
w_4 (DP)	t-test *p<0.01*	t-test *p<0.01*	t-test *p>0.01*	t-test *p<0.01*	t-test *p<0.01*	t-test *p<0.01*
w_5 (MAP)	W test *p<0.01*	W test *p<0.01*	W test *p>0.01*	W test *p<0.01*	W test *p<0.01*	W test *p<0.01*
w_6 (HR)	W test *p<0.01*	W test *p<0.05*	W test *p>0.01*	W test: *p>0.01*	W test *p>0.01*	W test *p>0.01*
w_7 (CBFV)	t-test *p<0.01*	W test *p<0.01*	W test *p<0.01*	W test *p<0.01*	W test *p>0.01*	W test *p<0.01*
w_8 (RI)	t-test *p>0.01*	t-test *p<0.01*	t-test *p>0.01*	t-test *p<0.01*	t-test *p>0.01*	t-test *p<0.01*
w_9 (PI)	t-test *p>0.01*	W test *p<0.01*	W test *p>0.01*	W test *p<0.01*	W test *p>0.01*	W test *p<0.01*
w_{10} (d)		W test *p<0.01*				
w_{11} (SaO_2)	W test *p>0.01*	W test *p<0.01*	W test *p>0.01*	W test *p<0.01*	W test *p>0.01*	W test *p<0.01*
w_{12} ($EtCO_2$)		t-test *p<0.01*				

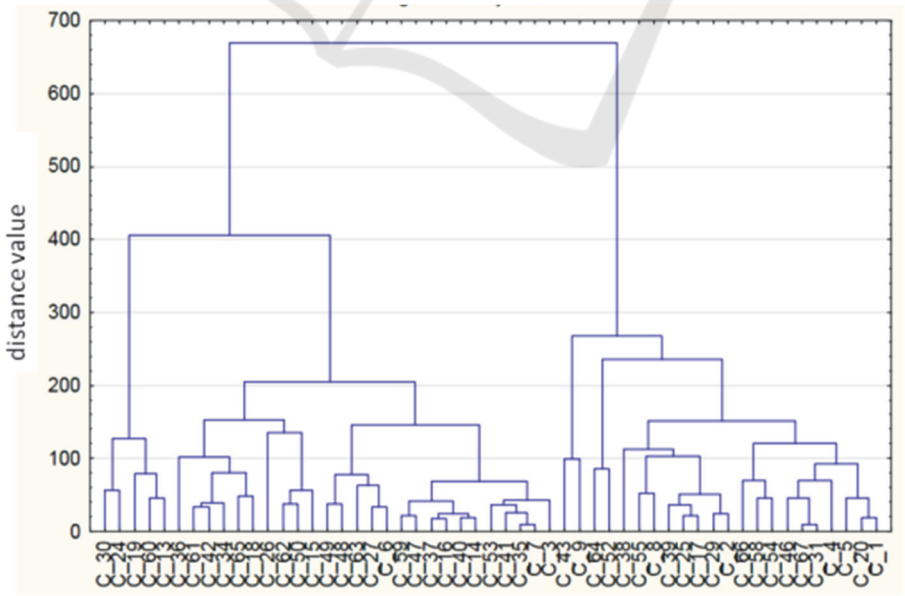

Figure 1: Data selection using a tree diagram (complete linkage, Chebyshev distance) on the left and right cluster. Symbols from C_1 to C_67 are consecutive numbers of data measurements. Symbols C_10, C_11, C_21, C_22, C_32, C_33, C_44, C_45, C_56 and C_57 are empty and do not take part in the analysis. There are results of data pre-processing.

The analysis showed that $\Delta_{13}ccTQ^{left\ cluster}$ depends on heart rate and pulsatility index changes:

$$\Delta_{13}ccTQ^{left\,cluster} = f_{left}(\Delta_{13}HR, \Delta_{13}PI) \quad (6)$$

The extract model function is as follows:

$$\Delta_{13}ccTQ^{left\,cluster} = -1.374 \cdot \Delta_{13}HR - 59.858 \cdot \Delta_{13}PI + 7.243 \cdot 10^{-2} \cdot \Delta_{13}HR^2 - 1.080 \cdot 10^{-5} \cdot \Delta_{13}HR^4 + \frac{67.012}{\Delta_{13}HR} + 2.184 \cdot 10^{-8} \cdot \Delta_{13}HR^5 - 0.1896 \quad (7)$$

$$\Delta_{13}HR \in R, \Delta_{13}HR \neq 0,$$
$$\Delta_{13}PI \in R, \Delta_{13}PI \neq 0$$

Figure 2 shows model function $\Delta_{13}ccTQ^{left\ cluster}$ which presents significant variability with changes of heart rate and pulsatility index. The control process undoubtedly is sophisticated. There are probably internal cross-couplings and cross-dependences. In consequence the function $\Delta_{13}ccTQ^{left\ cluster}$ shows a couple of maxima.

The $\Delta_{13}ccTQ^{right\ cluster}$ depends on heart rate, pulsatility index and mean cerebral blood flow velocity changes:

$$\Delta_{13}ccTQ^{right\,cluster} = f_{right}(\Delta_{13}HR, \Delta_{13}PI, \Delta_{13}CBFV) \quad (8)$$

One can see that $\Delta_{13}ccTQ^{left\ cluster}$ and $\Delta_{13}ccTQ^{right\ cluster}$ depend on partially overlapping variable sets, which suggest a different working principles. The obtained regression function and $\Delta_{13}ccTQ^{right\ cluster}$ is as follows:

$$\Delta_{13}ccTQ^{right\,cluster} = -\frac{51.386}{\Delta_{13}HR} - \frac{1.107}{\Delta_{13}PI} - 0.9281 \cdot \Delta_{13}HR - 7.428 \cdot \Delta_{13}CBFV - 5.975 \cdot 10^{-3} \cdot \Delta_{13}CBFV^3 + 0.4531 \cdot \Delta_{13}CBFV^2 + 0.43900 \quad (9)$$

$$\Delta_{13}HR \in R,\ \Delta_{13}HR \neq 0$$
$$\Delta_{13}CBFV \in R$$
$$\Delta_{13}PI \in R, \Delta_{13}PI \neq 0$$

Drawing the $\Delta_{13}ccTQ^{right\ cluster}$ requires using the 4-dimensional space. Instead we choose one of the variables ($\Delta_{13}PI$) as a parameter for the chart. Figure 3 shows a parametric graph of $\Delta_{13}ccTQ^{right\ cluster}$ changes for $\Delta_{13}PI$= -0.8.

$\Delta_{13}ccTQ^{right\ cluster}$ depends on heart rate changes ($\Delta_{13}HR$), mean cerebral blood flow velocity changes ($\Delta_{13}CBFV$) and pulsatility index changes ($\Delta_{13}PI$). Measured values of $\Delta_{13}ccTQ^{right\ cluster}$ were from -22.5 to 107.0 a.u.

Comparing $\Delta_{13}ccTQ^{left\ cluster}$ and $\Delta_{13}ccTQ^{right\ cluster}$ are observed two different modes of regulation: for $\Delta_{13}sasTQ>0$ and $\Delta_{13}sasTQ<0$ (see Figure 4). The $sasTQ^0$ is the initial value of sasTQ, before the experiment starts. The scale is expressed in the arbitrary units (a.u.).

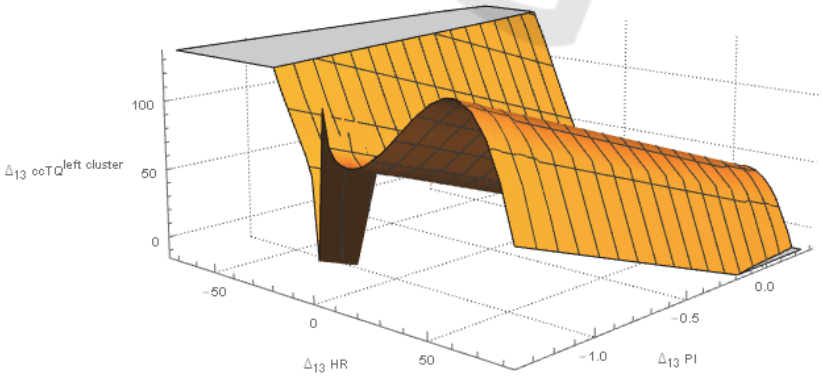

Figure 2: $\Delta_{13}ccTQ^{left\ cluster}$ [a.u.] versus $\Delta_{13}HR$ [beats/min] and $\Delta_{13}PI$ [1] drawn for an experimental range of variables, excluding $\Delta_{13}HR$=0.

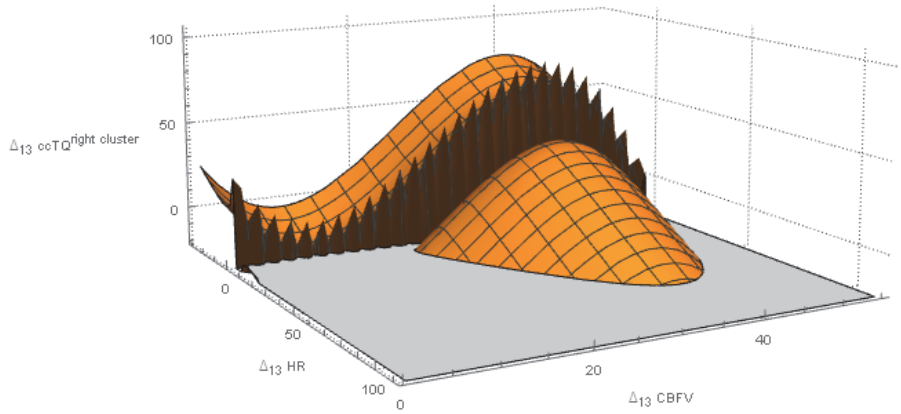

Figure 3: Parametric graph of $\Delta_{13}ccTQ^{right\ cluster}$ [a.u.] versus $\Delta_{13}HR$ [beats/min] and $\Delta_{13}CBFV$ [cm/s] drawn for experimental range of the variables and $\Delta_{13}PI$= -0.8, excluding $\Delta_{13}HR$=0.

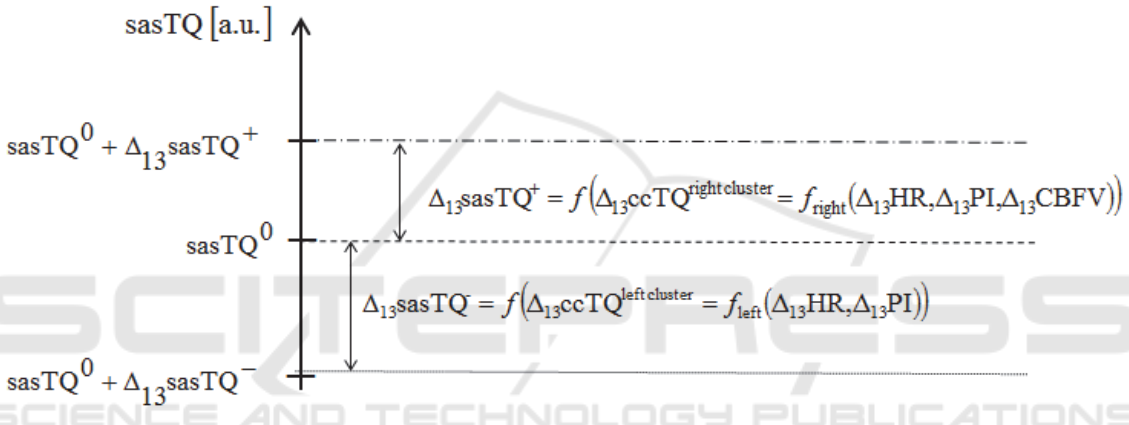

Figure 4: sasTQ response to apnoea. The initial value of $sasTQ^0$, as a result of the experiment, increases or decreases in dependence of $ccTQ^{right\ cluster}$ or $ccTQ^{left\ cluster}$. The scale is expressed as arbitrary units (a.u.).

As a result of the experiment with apnea, the initial value $sasTQ^0$ changes and reaches new level: $sasTQ^-$ which depends on heart rate changes and pulsatility index changes or $sasTQ^+$ which depends on heart rate changes, pulsatility index changes and mean cerebral blood flow velocity changes.

4 DISCUSSION

There are two main findings of this study: 1) the fast-variable component of SAS oscillations (from 0.5 to 5.0 Hz) is predominantly related to heart rate 2) there are two different subsets of cardiac SAS responses to breath-hold in humans.

The NIR-T/BSS model is based on the assumption that ccTQ is a result of heart-generated arterial pulsation (Frydrychowski et al., 2002), (Frydrychowski and Plucinski, 2007). Although the assumption is intuitive and in accordance with existing physiological knowledge (Linninger et al., 2005), (Wagshul et al., 2011), it has never been confirmed mathematically. Therefore, this study is the first to show that changes in ccTQ (plus and minus) depend on changes in heart rate (HR) and pulsatility index (PI).

During breath-hold, there is a powerful and differentiated activation of the sympathetic and parasympathetic nervous system (Foster and Sheel, 2005), (Paton et al., 2005), (Winklewski et al., 2013). Increased sympathetic drive may actually strengthen the myogenic response to elevated blood pressure through the addition of a neurogenic component (Cassaglia et al., 2008), (Cassaglia et al., 2009) and further protect the pial artery from vasodilation caused by apnoea-driven hypercapnia and subsequent acidosis (Winklewski et al., 2015b). Intense peripheral vasoconstriction, bradycardia, increased blood pressure and cerebral perfusion maintain adequate oxygenation of the heart and

brain at the expense of organs less sensitive to hypoxia. This increase in cerebral perfusion is partially independent of the partial pressure of CO_2 (Reis et al., 1997).

Differentiated heart-generated arterial pulsation in response to experimental breath-hold may partially explain the variability in tolerance to apnoea, hypercapnia and hypoxia observed in normal subjects.

The high within- and between-subject reproducibility and repeatability of NIR-T/BSS measurements have been demonstrated earlier (Frydrychowski et al., 2002). NIR-T/BSS, like NIRS, allows for direct within-subject comparisons (Frydrychowski et al., 2002), (Wagner et al., 2003). As long as changes from baseline values are analysed, high between-subject reproducibility is observed. However, measurements with the use of infrared light do not allow for direct comparisons between subjects due to differences in skull bone parameters (Frydrychowski et al., 2002), (Wagner et al., 2003).

5 CONCLUSION

The analysis showed that Δ_{13}sasTQ>0 depends on heart rate changes (Δ_{13}HR), mean cerebral blood flow velocity changes (Δ_{13}CBFV) and pulsatility index changes (Δ_{13}PI) and Δ_{13}sasTQ<0 depends on heart rate changes (Δ_{13}HR) and pulsatility index changes (Δ_{13}PI). This finding indicates two different modes of regulation.

Using mathematical modeling, we verified the assumption that ccTQ is predominantly heart-determined. This is an important step in the further development of NIR-T/BSS technology toward its clinical application. Furthermore, the variable heart-generated arterial pulsation response to experimental breath-hold described in this study provides new insights into our understanding of the complex mechanisms governing adaptation to apnoea in humans. Finally, we propose a mathematical methodology that can be used in further clinical research aimed at the development of personalized markers that will enable better diagnosis.

REFERENCES

Cassaglia, P. A., Griffiths, R. I., Walker, A. M., 2008. *Sympathetic nerve activity in the superior cervical ganglia increases in response to imposed increases in arterial pressure*. American Journal of Physiology. Regulatory, Integrative and Comparative Physiology. 294: R1255–61.

Cassaglia, P. A., Griffiths, R. I., Walker, A. M., 2009. *Cerebral sympathetic nerve activity has a major regulatory role in the cerebral circulation in REM sleep*. Journal of Applied Physiology. 106: 1050–6.

Drake, R., Vogl, A. W., Mitchell, A. W. M., 2009. *Gray's Anatomy for Students*. Elsevier Health Sciences.

Everitt, B. S., Landau, S., Leese, M., 2001. *Cluster Analysis (Fourth ed.)*. Arnold, London.

Frydrychowski, A. F., Gumiński, W., Rojewski, M., Kaczmarek, J., Juzwa, W., 2002. *Technical foundations for noninvasive assessment of changes in the width of the subarachnoid space with near-infrared transillumination-backscattering sounding (NIR-TBSS)*. IEEE Transactions on Biomedical Engineering. 49, 887-904.

Frydrychowski, A. F., Pluciński, J., 2007. *New aspects in assessment of changes in width of subarachnoid space with near-infrared transillumination-backscattering sounding, part 2: clinical verification in the patient*. Journal of Biomedical Optics. 12, 044016.

Foster, G.E., Sheel, A.W., 2005. The human diving response, its function, and its control. Scandinavian Journal of Medical Science in Sports. 15, 3–12.

Jolly, T. A., Bateman, G. A., Levi, C. R., Parsons, M. W., Michie, P. T., Karayanidis, F., 2013. *Early detection of microstructural white matter changes associated with arterial pulsatility*. Frontiers in Human Neuroscience. 7, 782.

Kalicka, R., 2014. *Basics of data analysis*, Gdańsk University of Technology Publishing, Gdańsk.

Kalicka, R., 2013. *Mathematical Modeling of Physio logical Systems to Aid in Diagnosis and Therapy*. Academic Publishing House EXIT, Warsaw.

Kaźmierski, R., 2011. *Podręczniki diagnostyki ultrasonograficznej w neurologii*. Czelej.

Li, Z., Zhang, M., Xin, Q., Li, J., Chen, G., Liu, F., Li, J., 2011. *Correlation analysis between prefrontal oxygenation oscillations and cerebral artery hemodynamics in humans*. Microvascular Research. 82, 304-10.

Linninger, A. A., Tsakiris, C., Zhu, D. C., Xenos, M., Roycewicz, P., Danziger, Z., Penn, R., 2005. *Pulsatile cerebrospinal fluid dynamics in the human brain*. IEEE Transactions on Biomedical Engineering. 52, 557–565.

Mazur, K., Kalicka, R., 2014. *Modeling of subarachnoid space width changes caused by blood circulation in brain vessels*. Proceedings of the Twentieth National Conference on Applications of Mathematics in Biology and Medicine.

Paton, J. F., Boscan, P., Pickering, A.E., Nalivaiko, E., 2005. *The yin and yang of cardiac autonomic control: vago-sympathetic interactions revisited*. Brain Research Reviews. 49, 555–565.

Reis, D. J., Golanov, E. V., Galea, E., Feinstein, D. L., 1997. *Central neurogenic neuroprotection: central neural systems that protect the brain from hypoxia and*

ischemia. Annals of the New York Academy of Sciences. 835, 168-86.

Stanisz, A., 2007. *Comprehensible statistics course using STATISTICA.PL - examples from medicine, vol. 1. Basic Statistics, vol. 2. Linear and non-linear models, vol. 3. Multidimensional Analyses*. StatSoft, Krakow.

Wagner, B.P., Gertsch, S., Ammann, R.A., Pfenninger, J., 2003. *Reproducibility of the blood flow index as noninvasive, bedside estimation of cerebral blood flow*. Intensive Care Medicine. 29, 196–200.

Wagshul, M. E., Eide, P. K., Madsen, J. R., 2011. *The pulsating brain: A review of experimental and clinical studies of intracranial pulsatility*. Fluids Barriers CNS. 8, 5.

Winklewski, P. J., Kot, J., Frydrychowski, A. F., Nuckowska, M. K., Tkachenko, Y., 2013. *Effects of diving and oxygen on autonomic nervous system and cerebral blood flow*. Diving and Hyperbaric Medicine Journal. 43, 148-56.

Winklewski, P. J., Gruszecki, M., Wolf, J., Swierblewska, E., Kunicka, K., Wszedybyl-Winklewska, M., Guminski, W., Zabulewicz, J., Frydrychowski, A. F., Bieniaszewski, L., Narkiewicz, K.. 2015. *Wavelet transform analysis to assess oscillations in pial artery pulsation at the human cardiac frequency*. Microvascular Research. 99, 86-91.

Winklewski, P. J., Barak, O., Madden, D., Gruszecka, A., Gruszecki, M., Guminski, W., Kot, J., Frydrychowski, A. F., Drvis, I., Dujic, Z., 2015 *Effect of Maximal Apnoea Easy-Going and Struggle Phases on Subarachnoid Width and Pial Artery Pulsation in Elite Breath-Hold Divers*. PLoS One. 10, e0135429.

Winklewski, P. J., Tkachenko, Y., Mazur, K., Kot, J., Gruszecki, M., Guminski, W., Czuszynski, K., Wtorek, J., Frydrychowski, A. F., 2015. Sympathetic Activation Does Not Affect the Cardiac and Respiratory Contribution to the Relationship between Blood Pressure and Pial Artery Pulsation Oscillations in Healthy Subjects. PLoS One. 10(8):e0135751.

Wszedybyl-Winklewska, M., Wolf, J., Swierblewska, E., Kunicka, K., Gruszecki, M., Guminski, W., Winklewski, P. J., Frydrychowski, A. F., Bieniaszewski, L., Narkiewicz, K., 2015. *Pial artery and subarachnoid width response to apnoea in normal humans*. Journal of Hypertension. 33, 1811-7; discussion 1817-8.

SOURCES OF FUNDING

This work was partially supported by funds of Faculty of Electronics, Telecommunications and Informatics, Gdańsk University of Technology.